SELF-FIELD AC POWER DISSIPATION IN HIGH-T_C SUPERCONDUCTING TAPES AND A PROTOTYPE CABLE

S. A. Awan and S. Sali

University of Newcastle upon Tyne
Department of Electrical and Electronic Engineering
Merz Court, Newcastle upon Tyne, NE1 7RU, United Kingdom

Abstract—The measured self-field AC power dissipation in superconducting BiSrCaCuO-2223/Ag tapes and a prototype cable is cable is compared with theoretical models. A brief overview of the theoretical background for AC loss calculations in superconductor tapes with different geometrical shapes is also discussed. New models for the harmonic components of the fundamental frequency and the current dependent non-linear inductance are also derived. It is shown that the latter models can be used to estimate current distribution and the variation of flux penetration in superconducting tapes. Two separate experimental apparatus were designed and constructed for measurements on tapes and prototype cable systems. The observed losses in tapes are reasonably well described by models based on the Critical State Model (CSM). In contrast, the measured losses in the prototype cable are found to be a factor of approximately two higher the predicted values. Further investigations showed that this may be due to inhomogeneous contact resistance between individual tapes and the current joints and the variation in critical current density (J_C) distribution between tapes. The significance of current dependence of the loss component, inductive quadrature component, phase error in measurements and the definition of the critical current in the prototype cable are also discussed.

1 Introduction

2 Theory

3 Experimental Details

1. INTRODUCTION

There has been considerable interest recently in characterising the self-field AC dissipation response of both high temperature superconducting (HTS) tapes and prototype cables [1]. Numerous studies carried out on mono filament tapes have shown that hysteretic energy dissipation can be accurately measured using a modified four-probe technique employing a small loop in the voltage leads so that the external magnetic flux in close proximity to the HTS conductor is sampled [2–5]. In contrast, multi-filament tapes have been studied only briefly [6]. In the first part of this paper therefore we discuss the observed power dissipation in 7, 19, 37 and 49-filament tapes in the frequency range 32–256 Hz. In the second part of the paper AC loss measurements on an insulated two layer helical prototype superconducting cable are compared with a theoretical model Similar to the small sample superconducting tapes, the position of the voltage contacts was also found to be critical for accurate loss measurements in a prototype conductor. In addition, there are other factors such as current distribution, phase error and contact resistance between the tapes and the current joints in a cable system which make such measurements particularly complex compared with the isolated samples. The significance of these factors on the observed losses and how their influence was minimized for accurate and reproducible measurements is also detailed. There are currently several research groups in the World who are actively involved in AC loss measurements on prototype superconducting cables [1, 7–9]. The observed losses in the two layer prototype conductor discussed in this paper are also compared, in addition to theoretical models, with measurements reported by these groups.

The goal of the work described in this paper is to present an analysis of the influence of various parameters such as current, frequency, thermal cycling, phase error and contact resistance on the self-field AC response of superconducting tapes and a short length prototype cable.

2. THEORY

There are two alternative but equivalent methods available for calculating the losses in superconducting materials analytically. Firstly, the loss per unit length can be determined by calculating the magnetic field distribution. and thus taking its average product with the applied field over a cycle. Alternatively, the losses may be evaluated from the average product of the local electric field and the applied transport current. However, as is standard in electromagnetic problems, depending on geometry and given applied conditions, different methods can be employed for better efficiency. Thus, using the latter method, in this section a brief overview of the self-field AC loss calculations in elliptical and strip geometry superconductors are described. In addition, new models for the harmonic components of the fundamental frequency and current dependent non-linear inductance are also derived by extending the previous expressions.

2.1. Elliptical Conductor

For an applied transport current $I_0(t) = I_{pt}\cos(\omega t)$ in the axial z-direction the current distribution in an elliptical superconductor during the descending half of the cycle $-I_{pt} \leq I_0 \leq I_{pt}$, consists of three regions with $J = 0$, $J = \pm J_c$, where ω is the angular frequency. The total current in the conductor during the half cycle is then given by [10]

$$I_0(t) = \frac{I_c}{a^2}\left[2c^2(t) - c_0^2 - a^2\right] \equiv I_{pt}\cos(wt) \tag{1}$$

where I_c is the critical current, a is the major axis dimension in the x-direction, c_0 is the maximum field penetration depending on the peak applied current I_{pt}, and $c(t)$ is the 'instantaneous' penetration of the reversing front, given by

$$c(t) = a\sqrt{1 + \frac{\beta}{2}[\cos(\omega t) - 1]} \tag{2}$$

where the reduced current $\beta = I_{pt}/I_c$. Therefore, the time average power dissipation in the conductor may be defined by

$$P = \frac{1}{T}\oint_T I_0(t) \cdot E(t)dt \quad (Wm^{-1}) \tag{3a}$$

or equivalently

$$P = \frac{1}{T} \oint_T I_0(t) \frac{d}{dt} \left(\lim_{x \to \infty} \int_0^x B dx \right) dt \tag{3b}$$

where T is the period of the applied current. The term in the brackets of (3b) represents the total flux change, ϕ, between the electric line in the conductor and the return conductor. As observed by Norris [10], the total flux change can be calculated by the superposition of the magnetic field distributions at peak minus twice the distribution at a given lower field, such that

$$\phi(x, t) \approx \frac{\mu_0 I_c}{\pi a^2 (1 + \xi)} \left[x \sqrt{x - c^2(t)(1 - \xi^2)} \right.$$
$$\left. - c^2(t) \ln \left(\frac{x + \sqrt{x - c^2(t)(1 - \xi^2)}}{c(t)} \right) \right] \tag{4}$$

which is similar to the expression given by Yang et al. [4] except for the aspect ratio $\xi = b/a$, where b is the minor axis dimension. For the case where $x \to \infty$ as in (3b), it may be seen from (4) that the flux converges to an asymptotic value given by

$$\phi(x \to \infty, t) = \frac{\mu_0 I_c}{\pi a^2} \left(-c^2(t) \ln[c(t)] \right) \tag{5}$$

The loss per unit length can be calculated by substituting (1) and (5) into (3b), which leads to

$$P = \frac{\mu_0 I_{pk}^2 f}{2\pi} \int_0^x \cos(\omega t) \sin(\omega t) \ln \left[1 + \frac{\beta}{2} (\cos(wt) - 1) \right] dt \tag{6}$$

and after some manipulation this leads to [10]

$$P = \frac{\mu_0 I_c^2 f}{2\pi} [(2 - \beta)\beta + 2(1 - \beta)\ln(1 - \beta)] \left(W m^{-1} \right) \tag{7}$$

It is interesting to note that the losses predicted by (7) are independent to the aspect ratio, and thus also apply to a *circular* conductor. Although (7) gives the magnitude of the loss variation with applied current, it cannot be used to predict the instantaneous variation. The instantaneous axil electric field during the descending half of the cycle

can be determined by differentiating (4) with respect to time, which gives

$$E^{\downarrow}(x,t) = \frac{\mu_0 I_{pt}\omega}{2\pi}\left[\sin(\omega t)\ln\left[\frac{x + \sqrt{x^2 - c^2(t)\,(1 - \xi^2)}}{c(t)}\right]\right] \tag{8}$$

where $E^{\downarrow}(x,t) = 0$ for $|x| \le c(t)$ since there is no flux change between the electric center line and the contour $c(t)$, therefore (8) is only valid for $|x| \ge c(t)$. Similarly, for the ascending half of the cycle, $E^{\uparrow}(x,t) = E^{\downarrow}(x,T-t)$ where $(m + 1/2)T \le t \le mT$. The corresponding power dissipation may be calculated, with $x = a$ in (8), thus substituting (8) into (3a)

$$P = \frac{2}{T}\int_0^{T2} I_0(t) \cdot E^{\downarrow}(a,t)dt \tag{9}$$

Although the analytical solution of this integral is complex, it can be modelled numerically. Clearly the power dissipation given by (7) and (9) should in principle be equivalent. However, at $\beta = 0.1$ for example, the difference between the losses predicted by (7) and (9) is found to be approximately an order of magnitude. This is due to $E^{\downarrow}(x,t)$ being restricted to the value at $x = a$, i.e., the total flux change between the electric center line and the surface of the conductor. However, the losses predicted by (9) rapidly approach the asymptotic values, given by (7) when $x \to 3a$, as discussed in [4]. A further important feature of (8) is that the influence of the fundamental frequency on the measured electric field can also be studied. As it can be seen from (9), only the fundamental harmonic component of the electric field contributes to the *real* hysteretic power dissipation in the conductor, and it can easily be shown using (9) that the remaining odd harmonics of the fundamental do not contribute to power dissipation, i.e., $P = E_1 I_{rms}$. In contrast, all the odd harmonics contribute to the quadrature component of the surface electric field. The influence of the harmonics can readily be evaluated using Fourier analysis. Assuming that the measured electric field $E(t)$ has the from

$$E(t) = \sum_{k=1}^{\infty}\left[E_k\cos(k\omega t) + E_k'\sin(k\omega t)\right] \tag{10}$$

where E_k and E_k' are the *in-phase* and *quadrature* fourier components of the measured electric field [11]

$$E_k = \frac{2}{\pi}\int_0^x E^{\downarrow}(x,t)\cos(k\omega t)dt \tag{11}$$

$$E'_k = \frac{2}{\pi} \int_0^x E^\downarrow(x,t)\sin(k\omega t)dt \qquad (12)$$

where $E^\downarrow(x,t)$ is given in (8). Since $E^\downarrow(x,t)$ is an odd function k in (11) and (12) may be replaced by $k = 2n + 1$ where $n \geq 0$. Further, it should be noted that the quadrature electric field (12), consists of two distinct components due to *internal* and *external* inductive flux linkage with measuring voltage leads. Alternatively, the second term in the brackets of (10) may be rewritten as

$$E'_T(x,\beta) = j\omega I_{rms}\left(I_i(\beta) + L_e(x)\right) \qquad (13)$$

where $E'_T(x,\beta)$ is the *total* (i.e., summation of all k-th odd harmonic components) quadrature electric field, $L_i(\beta)$ and $L_e(x)$ are the equivalent internal and external inductance formed between the electric center in the HTS conductor and the axial closing line of the measuring voltage leads. Additionally, there wire also be a finite contribution to $E'_T(x,\beta)$ from the *geometric inductance* of the conductor, $L_0 \cong \mu_0/8\pi (Hm^{-1})$. However, even for a small loop in the voltage leads $L_0 \ll (L_i + L_e)$. Expressions for $L_i(\beta)$ and $L_e(x)$ in a homogenous elliptical conductor are given in [12, 13].

2.2. Thin Strip Conductor

Although the self-field AC losses in a thin strip (width $2a$ and thickness $d \to 0$) can also be evaluated using (3), the analytical calculation of the current and magnetic field distributions is more complex than the elliptical geometry. However it is possible to use conformal mapping and the method of images to obtain the current and magnetic field distribution, such that [10, 14, 15]

$$J_z(x,\beta) = \begin{cases} J_{c'} & -a < x \leq -c_0 \\ \dfrac{2J_c}{\pi}\tanh^{-1}\left(\sqrt{\dfrac{a^2-c_0^2}{a^2-x^2}}\right), & -c_0 < x < c_0 \\ J_{c'} & c_0 \leq x < a \end{cases} \qquad (14)$$

where $J_c = I_c/2a$ is the critical current density per unit width of the strip, and $c_0 = a\sqrt{1-\beta^2}$ is the maximum field penetration as mentioned earlier. The magnetic field distribution in the strip is given

by [10, 14, 15]

$$B_y(x, \beta) = \begin{cases} 0, & |x| < c_0 \\ \dfrac{\mu_0 J_c}{\pi} \tanh^{-1}\left(\sqrt{\dfrac{x^2 - c_0^2}{a^2 - c_0^2}}\right), & c_0 < x < a \\ \dfrac{\mu_0 J_c}{\pi} \tanh^{-1}\left(\sqrt{\dfrac{a^2 - c_0^2}{x^2 - c_0^2}}\right), & x > a \end{cases} \tag{15}$$

An interesting feature of (15) is that *logarithmic* singularity occurs for $x \to \pm a$. However, in amore accurate analysis this would be avoided by taking into account the finite thickness of a practical strip [10, 15]. Clearly, due to symmetry (15) is also valid for $x < 0$, and may be rewritten as $x \cdot B_y(x)/|x|$. It is now possible to calculate the self-field AC dissipation in a thin strip conductor by substituting (14) and (15) into (3a), so that

$$P = \frac{1}{T} \int_0^T dt \int_{-a}^a J_c \frac{d\phi(x, t)}{dt} dx \tag{16}$$

since $J = J_c$ for $|x| > c_0$, and $B_y(x) = 0$ for $|x| < c_0$. Evaluating the integrals in (16) and after some manipulation gives the power loss per unit length in a strip conductor [10]

$$P = \frac{\mu_0 I_c^2 f}{\pi} \left[(1 + \beta)\ln(1 + \beta) + (1 - \beta)\ln(1 - \beta) - \beta^2\right] \tag{17}$$

Similar to (8), the instantaneous axial electric field is found to be [11]

$$E^\downarrow(x, t) = \frac{\mu_0 I_c \omega \beta}{4\pi} \sin(\omega t)\ln\left[\frac{x + \sqrt{x^2 - c^2(t)}}{c(t)}\right] \tag{18}$$

where $c(t) = a\sqrt{1 - (\beta - \beta(t))^2/4}$, $\beta(t) = \beta\cos(\omega t)$, and $E^\uparrow(x, t) = E^\downarrow(x, T - t)$ such that $(m + 1/2)T \le t \le mT$. Thus, substituting (18) into (9), it can readily be shown that the numerical solution to this integral is within 10% of the values given by (17) for $x \ge 3a$. The influence of the harmonics of the fundamental on the inphase and quadrature components of the electric field for the strip conductor can also be determined by substituting (18) into (11) and (12). For the quadrature electric field the corresponding internal and external components for a thin strip conductor can be evaluated using

$$L_T(x, \beta) = \frac{1}{I_{rms}} \int B_y(x, \beta) dx \tag{19}$$

where $B_y(x, \beta)$ is given in (15), and the total equivalent inductance may be rewritten as

$$L_T(x, \beta) = L_i(\beta) + L_e(x, \beta) \tag{20}$$

where the internal component of the non-linear current dependent inductance is found to be [16]

$$L_i(\beta) = \frac{\mu_0}{4\pi\beta} \left[(1 + \beta)\ln(1 + \beta) + (1 - \beta)\ln(1 - \beta) \right] \tag{21}$$

and for the external component, we find

$$L_e(x, \beta) = \frac{\mu_0}{4\pi\beta} \begin{bmatrix} u\ln\left(\dfrac{\eta + \beta}{\eta - \beta}\right) + 2\beta\ln\left(\dfrac{\eta + u}{1 + \beta}\right) + \ln\left(\dfrac{u - 1}{1 + u}\right) \\[2mm] \ln\left(\dfrac{\beta(\beta + \eta) - (1 + u)}{(1 - u) - \beta(\beta + \eta)}\right) - \ln(1 - \beta^2) \end{bmatrix} \quad \beta < 1 \tag{22}$$

where $u = x/a$, x is the loop width of the voltage leads and $\eta = \sqrt{u^2 + \beta^2 - 1}$. There are two important aspects which should be noted from (22). Firstly, it is interesting to observe that the external component of the inductance is current dependent, which is in sharp contrast with the elliptical conductor [12]. And secondly, as mentioned earlier, the magnetic field approaches a logarithmic singularity as $x \to \pm a$, which consequently, is also observed in the external – but not the internal – equivalent inductance for the strip conductor when $\beta \to 1$.

3. EXPERIMENTAL DETAILS

The critical current of the tapes was measured by a standard four-probe method using a $1\mu\text{Vcm}^{-1}$ electric field criterion (at 77 K, 0T). The I_c and other parameters of the multi filamentary tapes are given in Table 1.

The two layer prototype superconducting cable was fabricated by helically wrapping 24 tapes per layer on a Cu former of 25.4 mm diameter. The overall length of the tapes was 700 mm, resulting in an active 450 mm length conductor. Although both layers were wrapped at a pitch angle of 315°, the upper layer had an opposite helicity to ensure that the resultant magnet c field had only a tangential component. In addition, the two layers were separated by a 0.1 mm thick paper tape insulation.

The self-field AC loss measurement system used to characteries the short length samples is shown in Fig. 1. The oscillator output

Table 1. Critical current and parameters for the multi-filament tapes.

Sample	$I_C(A)$	Tape Dimensions (mm)		Core Dimensions (mm)		$\xi = b/a$
		$2a_0$	$2b_0$	$2a$	$2b$	
MF-7	15.4	2.75	0.31	2.48	0.18	0.07
MF-19	11.6	4.42	0.33	4.12	0.23	0.06
MF-37	10	2.7	0.22	1.9	0.19	0.1
MF-49	7.5	2.8	0.25	2.14	0.12	0.056
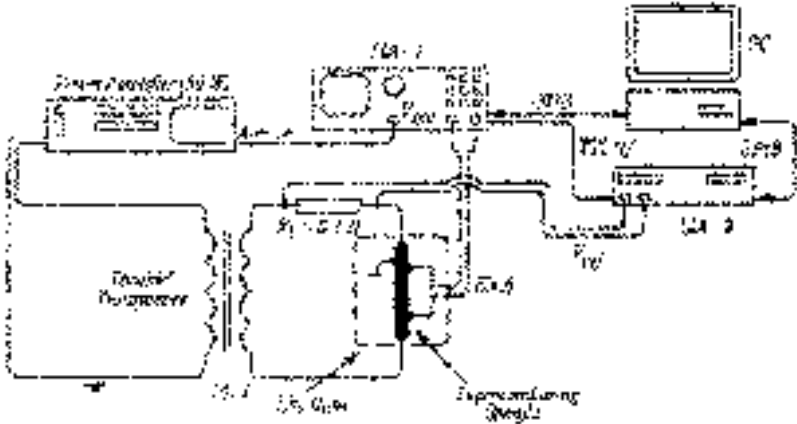
Figure 1. Experimental set-up for self-field SC loss measurements on superconducting Bi-2223/Ag tapes.

of the Lock-in Amplifier-1 (LIA-1) is used to supply the transport AC current to the sample via a $50\,W$ power amplifier and a $100\,VA$ toroidal current transformer. The output of the transformer is connected to the superconducting sample in series with a $30\,W$ non-inductive reference resistor, which is also attached to a heat sink. Phase of the applied transport current is measured from across the reference resistor using a second dual phase LIA-2. The LIA-2 is operated in an external mode with a TTL reference signal from LIA-1. The sample holder was designed to ensure minimal field effects on the sample and to reduce the impedance of the circuit connected to the output of the transformer. The copper current leads were the same width as the sample, and were directly soldered to the ends of the specimen. Precautions were taken to avoid noise interference, ground loops and common mode signals. Measurements were carried out at $77\,K$ for frequencies in the
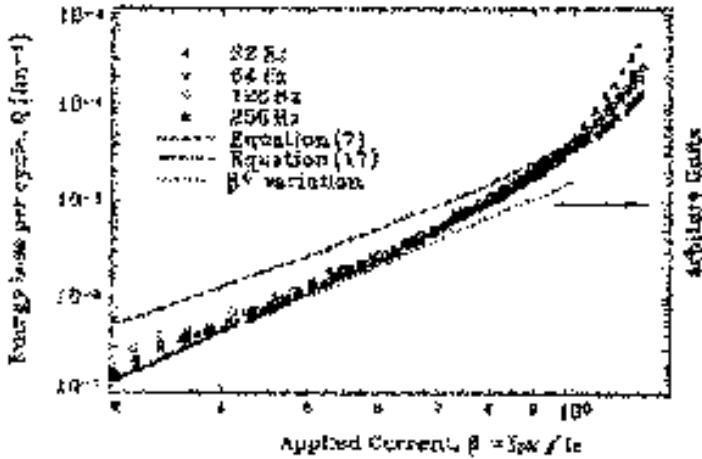
Figure 2. Comparison of energy dissipation in the 7-filament tape at several frequencies. Note the function β^4 and equation (17), illustrating exact strip type dissipation measured in the sample.

range of 32 to 256 Hz and for current up to 30 A_{pk}. The sensitivity of our apparatus was better than $10\,nV$, and the reproducibility of the measurements was found to be within 2%.

The single phase prototype conductor was characterised using a second second set-up, which in principal is similar to that shown in Fig. 2, except for the power amplifier and transformer. The main modifications included a 700 A_{pk} (3 kVA) floating earth power supply (which could deliver 9 kVA for a short 20 second pulse operation), oil cooled 1 mΩ (490 W) non-inductive resistor, cable assembly holder and an appropriate current leads design for both current capacity and minimum impedance load. Similar to the short sample apparatus, phase of the applied transport current was also determined from the non-inductive resistor. Both experiments were fully automated using Turbo Pascal 7.0 and an IEEE-GPIB interface with a PC for data acquisition.

4. RESULTS AND DISCUSSION

The self-field AC energy loss per cycle in the 7 filament tape (MF-7) for 32–256 Hz versus β using a 7.5 mm loop in the voltage leads is shown in Fig. 2. The critical current of MF-7 tape was 15.4 A, as shown in Table 1. The dashed and solid lines shown in the graph are given by (7) and (17), respectively, where $Q = P/f$ in ($J/m/cycle$). It is clear from
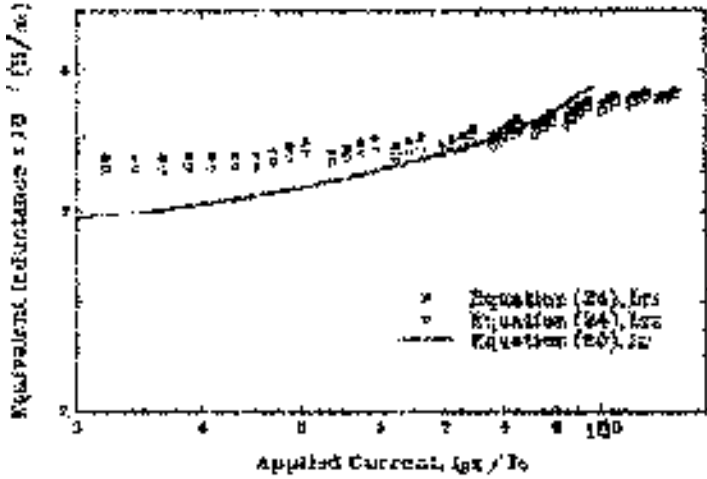
Figure 3. Measured and calculated equivalent inductance variation with applied current in the 7-filament tape at 256 Hz. second set of data (L_{T2}) demonstrates the reproducibility of the measurements to within 2%.

Fig. 2 that the observed energy loss per cycle for applied current $\beta \leq 1$ is frequency independent, i.e., hysteretic. In this region of applied current, good agreement between the measured and calculated values for a thin strip conductor (17) can be seen. For $\beta \leq 1$ the measured losses for all frequencies demonstrate, in addition to the accuracy of the magnitude of the losses, one further significant feature. For low applied current (17) can be rewritten as

$$Q \approx \frac{\mu_0 I_c^2}{6\pi} \left[\beta^4 \left(1 + \frac{12\beta}{5} \right) \right] \approx \frac{\mu_0 I_c^2}{6\pi} \beta^4 \tag{23}$$

This is also plotted in Fig. 2 as a dotted line. Although the measured and calculated losses show good agreement with β^4 current dependence, there is a marked deviation for higher applied currents $\beta > 0.7$. It is this which is particularly significant, because the *measured losses* follow very closely the exact variation of the *predicted losses* given by (17). For $I_{pk} > I_C$ the observed losses show a highly non-linear flux flow behavior, such that $Q \propto \beta^n$ where the exponent n varies between 8–10 for the given range of frequencies.

　　Fig. 3 shows the corresponding quadrature electric field measured in the MF-7 tape for the 256 Hz data (including a second set of data to highlight reproducibility of the measurements), converted to an

equivalent inductance, such that

$$L_T(x, \beta) = \sqrt{2}E'/\omega\beta I_c \quad (Hm^{-1}) \tag{24}$$

where $x = (7.5 + a_0)$ mm, and the value for a_0 (half width of the tape) is given in Table 1. Although a slight difference in the equivalent inductance can be seen on a log-log plot in Fig. 3, it should be noted that the actual difference between the two sets of data (L_{T1}, and L_{T2}) is merely 2%. In contrast with a normal conductor where the equivalent inductance would be expected to show a constant value with applied current (assuming negligible skin effect), a clear variation in the measured values can be seen with β. The solid line in Fig. 3 shows the calculated values given by (20). As it can be seen from Fig. 3, the agreement between measured and predicted values is reasonably good. For example, at $\beta = 0.35$ the difference between the measured and calculated values is found to be approximately 10%. In addition, the exponent variation of the measured and predicted values is found to be $n = 0.3$ and $n = 0.45$, respectively for $0.7 \leq \beta < 1$, corresponding to $E' \propto I_{pk}^{1.3}$ for the measured inductive electric field. In comparison with a normal conductor, the quadrature electric field would be expected to show a $n = 1$ current dependence. Since the overall measured self-field response of the 7 filament tape showed good agreement with calculated values, this suggests that the tape is behaving as a true thin strip conductor with homogeneous J_c distribution and flux penetration properties accurately described by the CSM.

Fig. 4 shows the reduced power dissipation in MF-I9, 37 and 49 filament tapes at 64 Hz against β, such that $P_r = P/I_c^2$, where P is given in (7). Although a finite difference between the measured losses and those predicted by (7) can be seen, it is clear that the self-field dissipation response of the three tapes is more closely modelled by the elliptical (7) rather than the thin strip (17) geometry. This is in sharp contrast with MF-7 tape discussed earlier. The significant and contrasting self-field losses observed in the 7 filament tape and the remaining multi-filamentary tapes need to be considered in more detail. These distinct differences may be explained in terms of the variation of the self-field penetration into the core with β. The flux penetration in the MF-19 and 49 filament tapes, as indicated by the loss behavior, suggests that the filaments were self-field coupled (it should be noted that the filament in MF-19 and 49 did not show any bridging or connectivity in cross-sectional optical micrographs). However, the MF-37 tape showed extensive inter-filament connectivity, effectively resulting in a bulk mono-core geometry. As such, for the higher filament tapes, it is likely that the inner filament were shielded from the self-field for $I_{pk} < I_c$, and only for increasing I_{pk} more inner
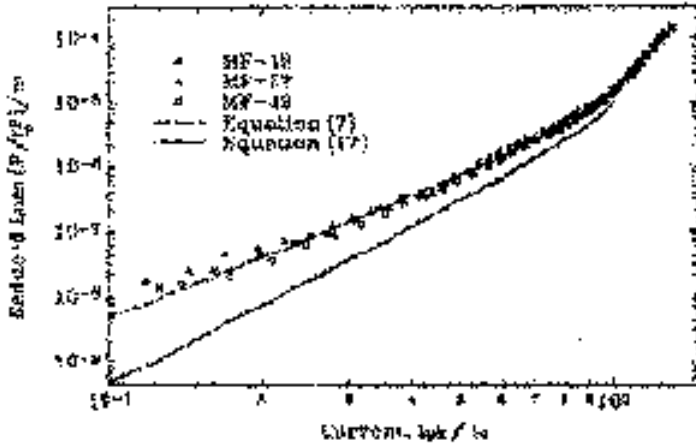
Figure 4. comparison of the reduced power dissipation in multifilament tapes at 64 Hz with calculated values for elliptical (7) and trip (17) conductors.

filaments begin to carry the transport current. In contrast, in the 7-filament tape the current flow is not restricted to the outer filament and may even have majority of the transport current flowing in the central portion of the tape.

The influence of thermal cycling on self-field AC losses is also an important consideration for practical applications. There are numerous possibilities which can result in a rapid cryogen boil-off device quench, leading to degradation of HTS material properties [17]. Although a thermal cycle may be defined in many ways, with various warm-up times, the thermal used here consisted of (A) measure the critical current and the losses in the sample after its first cool-down in LN_2, (B) allow LN_2 room temperature, and (C) remeasure the critical current and the losses in the sample after its second cool-down. Fig. 5 shows a comparison of the observed power dissipation at 128 Hz in MF-49 tape, discussed above, before and after being thermally cycled. After the second cool-down, the I_c of the tape showed a 10% drop to 6.8 A, which is a relatively large reduction for natural LN_2 boil-off [11]. As it can be seen from Fig. 5, the measured losses against I_{pk} are found to be higher in the thermally cycled case for the entire range of applied current. Therefore, the effects of thermal cycling may be considered as having a strong influence on the critical current of a tape, which in turn determines the level of dissipation in the tape.
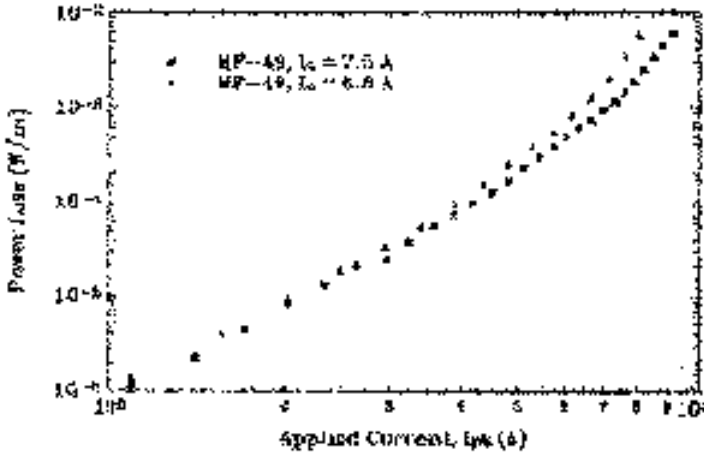
Figure 5. Influence of thermal cycling in a 49-filament tape at $128\,\mathrm{Hz}$. The $I_c = 7.5\,A$ (before) and $I_c = 6.8\,A$ (after) the thermal cycle.

5. PROTOTYPE SUPERCONDUCTING CABLE

The prototype superconducting cable consisted of an inner conductor with two layers of helically [11, 18] wrapped 7-filament BSCCO-2223/Ag tapes and a coaxial copper return. The inner and the return conductors were separated by paper insulation tape. The nominal i_c of individual tapes was $16\,A$ leading to a maximum critical current of $I_c = 768\,A$ for 48 tapes in the conductor. However, the measured critical current of the conductor was $I_c = 390\,A$, or a difference of approximately 50%. This is considered to be due to inhomogeneous contact resistance and possible mechanical damage during the fabrication of the conductor, leading to degradation in i_c of the individual tapes. Although two other types of conductors have also been measured – single layer and a non-insulated double layer using various voltage tap configurations [11] – the results reported here are for the double layer insulated conductor with four pairs of voltage contacts. Contacts (1, 2) were attached to two side-by-side tapes (following the helicity of the tapes in the upper layer) in the center of the conductor (to avoid edge field effects), and contacts (3, 4) were attached equidistance around the circumference of the conductor at the current joints [1]. The DC measurements using (1, 2) led to critical current values of $I_{c1} = 246\,A$ and $I_{c2} = 218\,A$, respectively. In contrast, measurements using (3, 4) were dominated by the resistance of the current joints, and as such the critical current of the conductor
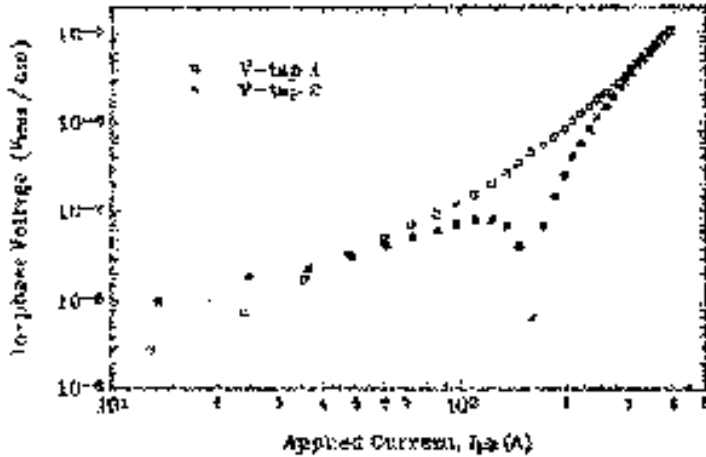
Figure 6. Measured in-phase voltage using contacts (1, 2) at $32\,\mathrm{Hz}$ against peak applied current.

could not be distinguished.

The corresponding in-phase voltage measured at $32\,\mathrm{Hz}$ (and at $77\,\mathrm{K}$) using (1, 2) is shown in Fig. 6. Although for contact (1) the measured voltage is found to show a $V \propto I^n$ where $n \cong 2$ dependence when $I_{pk} < 150\,A$, it is interesting to note that for contact (2) a large dip can be seen for a $\log|E|$ plot at $150\,A$. This latter effect is characteristic of a significant phase difference between current in the tape under test and the phase of the total applied transport current. An equivalent effect in individual tapes has recently been illustrated by Müller and Leslie [19]. As such, the main drawback of the electrical technique (when the voltage contacts are attached to individual tapes) is that since the phase and magnitude of the current flow through a given tape is unknown significant errors can occur in the observed losses. Therefore as suggested by Leghissa et al. [1] for 'average' power dissipation in the conductor it is more appropriate to perform measurements over the length of the conductor and to subtract the Ohmic contribution of the current pints from the measured voltage. The Ohmic contribution of the current joints can readily determined from DC measurements. The measured in phase and quadrature components for contacts (3, 4) are shown in Figs. 7 and 8. For $I_{pk} \geq 70\,A$ the in-phase and the quadrature components show a $n = 2$ and a $n = 1$ current dependence (illustrated by the solid lines). It is interesting to note that the quadrature components are effectively comparable to the in-phase components for the entire range of applied
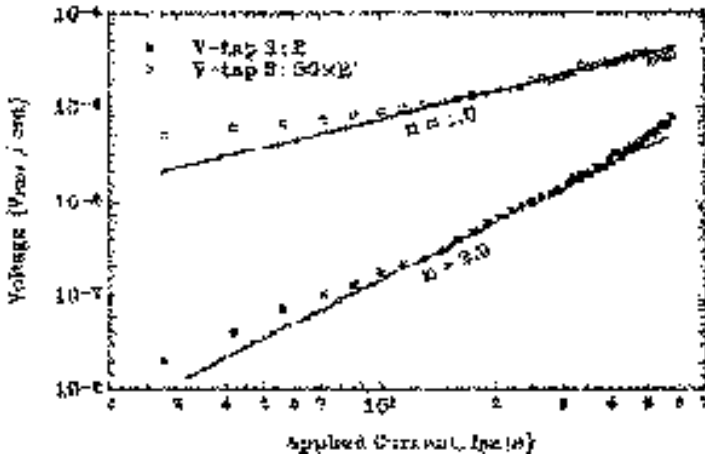
Figure 7. Measured in-phase and quadrature voltages using contact (3). The exponent variations are illustrated by the solid lines (the data for the quadrature component has been multiplied by factor of 50 for clarity in graph.
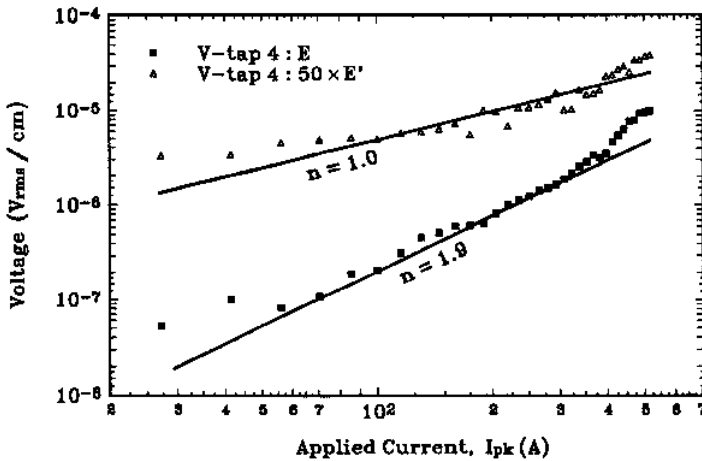

Figure 8. Measured in-phase and quadrature voltages using contact (4) against peak applied current.
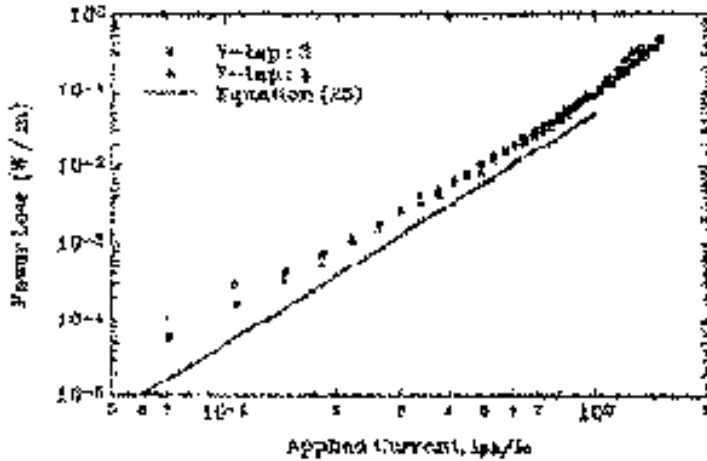
Figure 9. The corresponding measured and calculated power dissipation in the 2.5 KVA (417 A) two layer helical superconducting cable at 32 Hz against reduced applied current, where $I_c = 390\,A$.

current (the former components have been multiplied by a factor of 50 for clarity in the graphs). In contrast, the quadrature components are usually significantly larger than the in-phase components for measurements on individual tapes. This difference is as expected since edge field effects are minimal in a cylindrical geometry. For the in-phase components a relatively large deviation can be seen from the respective current dependencies for $I_{pk} < 70\,A$. This may be due to phase errors for small applied currents. Although the average critical current of the conductor could not be obtained from DC measurements for contacts (3, 4), it can be estimated from AC measurements. As it can be seen from Figs. 7 and 8, the measured in-phase voltage shows a sharper increase at approximately $390\,A$, i.e., a transition to flux flow regime such that the exponent changes from $n = 2$ to $n = 2.8$. It is considered that this represents the 'average' critical current of the conductor, such that $i_c = 8.1\,A$ per tape. This is in sharp contrast with the values measured using contacts (1, 2). It should be noted that due to different tapes having different transitions the highly non-linear flux flow behavior usually observed in individual tapes (with $n \to 20$) is 'smeared-out' in the cable resulting in $n = 2.8$.

The in-phase voltage measured using contacts (3, 4) converted to average power dissipation in the conductor against reduced applied current β is shown in Fig. 9. The solid line shown in the Fig. 9 is given

by [20]

$$P = \frac{\mu_0 I_c^2 f}{2\pi \delta_0^2} \left[(2 - \delta_0 \beta)\beta + 2(1 - \delta_0 \beta)\ln(1 - \delta_0 \beta) \right] \quad \left(Wm^{-1} \right) \quad (25)$$

where $I_c = 390\,A$ and $\delta_0 = 1 - a_0^2/a^2 = 0.147$ (with $a_0 = 12.7\,mm$ and $a = 13.75\,mm$ being the inner and outer radii of the conductor). Firstly, it is clear from Fig. 9 that a reasonably good reproducibility of the results to where $I_c = 390\,A$ and $\delta_0 = 1 - a_0^2/a^2 = 0.147$ (with $a_0 = 12.7\,mm$ and $a = 13.75\,mm$ being the inner and outer radii of the conductor). Firstly, it is clear from Fig. 9 that a reasonably good reproducibility of the results to within $\pm 10\%$ is obtained. And secondly, the measured losses show hysteretic I^3 dependence for $\beta \leq 1$. However, there is on average a factor of 1.9 difference in magnitude between the measured and calculated values for $0.2 \leq \beta \leq 1$. Further investigations on other cable cable showed that this may be due to inhomogeneous current distribution between the tapes as a result of the contact resistance at the current joints, or due to inter-tape current transfer. A further possibility may be the *simplicity* of the model given by (25), which does not take into account the helicity or the highly anisotropic electromagnetic properties of the superconducting tapes. Although Leghissa et al. [1] have also measured losses showing hysteretic I^3 dependence in a two layer conductor, a factor of 3 difference between the measured and calculated losses was observed. Furthermore, the cubic current dependence has also been observed by Fujikami et al. [9] in a two layer insulated conductor, though comparisons with a theoretical model were not included In contrast, for a two layer non-insulated conductor Gannon et al. [8] have observed a I^2 loss dependence, whereas Mukoyama et al. [7] find good agreement with theoretical predictions, though this is only achieved by homogenising current distribution with additional impedance insertion between the layers.

6. CONCLUSIONS

The observed self-field AC losses in multi-filamentary tapes and a prototype superconducting cable have been compared with theoretical models. The dissipation and inductance response of the 7-filament tape showed good agreement with models for a thin strip geometry. In contrast, the self-field losses observed in the 19, 37 and 49-filament tapes showed better agreement with the elliptical geometry. New theoretical models for the harmonic components of the fundamental frequency and the non-linear current dependent equivalent inductance

have also been presented. Thermal cycling of the 49-filament tape showed a reduction in the tape I_C, and a corresponding increase in the self-field AC losses.

The self-field losses observed in a two layer insulated prototype superconducting cable were found to show hysteretic I^3 dependence for $\beta \leq 1$. Furthermore, reproducibility of the measurements from two separate voltage contacts was found to be within $\pm 10\%$. However, the magnitude of the measured losses u as found to be a factor of approximately 2 higher than the calculated values. Possible explanations for this discrepancy were discussed. For voltage contacts attached to the current joints it was found that the critical current of the conductor can only be determined from AC measurements. Comparisons with results from other workers showed good agreement for the current dependence of the self-field AC power dissipation on similar conductor configurations.

ACKNOWLEDGMENT

REFERENCES

1. Leghissa, M., B. Fischer, B. Roas, et al., "Bi-2223 multifilament tapes and multistrand conductors for HTS power transmission cables," *IEEE Trans. Appl. Supercond.,* Vol. 7 No. 2, 355–358, 1997.

2. Campbell, A. M., "AC losses in high T_C superconductors," *IEEE Trans. Appl. Supercond.,* Vol. 5, No. 2, 682–687, 1995.

3. Pe, T., J. McDonald, and J. R. Clem, "Voltage-probe-position dependence and magnetic-flux contribution to the measured voltage in ac transport measurements: which measuring circuit determines the real losses?" *Proc. First Polish-U.S. Conf. High-T_c Supercond.,* Springer-Verlag, 1995.

4. Yang, Y., T. Hughes, C. Beduz, et al., "The influence of geometry on self-field AC losses of Ag sheathed PbBi2223 tapes," *Physica C,* Vol. 256, 378–386, 1996.

5. Ciszek, M., S. P. Ashworth, M. P. James, et al., "Self-field AC losses and critical currents in multitube Ag-Bi-2223 conductors," *Supercond. Sci. Technol.,* Vol. 9, 379–384, 1996.

6. Mele, R., G. Crotti, L. Gherardi, et al., "Analysis of AC loss behavior in BSCCO tapes with different core geometries," *IEEE Trans. Appl. Supercond.,* Vol. 7, No. 2, 1351–1354, 1997.

7. Mukoyama, S., K. Miyoshi, H. Tsubouti, et al., "50 in long high-T_C superconductor for power cables," *IEEE Trans. Appl. Supercond.,* Vol. 7, No. 2, 1069–1072, 1997.

8. Gannon, J. J. Jr., A. P. Malozemoff, M. J. Minot, et al., "AC losses in Bi-2223 composite tapes," *Adv. Cryogen. Eng.,* Vol. 40, 45–52, Plenum, New York, 1994.

9. Fujikami, J., N. Shibuta, K. Sato, et al., "Effective reduction of AC loss in HTSC cable conductor," *Adv. Supercond. VII,* 1195–1198, Springer-Verlag, Tokyo, 1995.

10. Norris, W. T., "Calculation of hysteresis losses in hard superconductors carrying ac: isolated conductors and edges of thin sheets," *J. Phys. D,* Vol. 3, 489–507, 1970.

11. Awan, S. A., "Self-field AC losses in high-T_C superconducting BSCCO-2223/Ag tapes and prototype conductors," Ph.D. thesis, University of Newcastle upon Tyne, UK, April 1997.

12. Awan, S. A., S. Sail, C. M. Friend, and T. P. Beales, "Transport AC losses and nonlinear inductance in high temperature superconductors," *IEE Elec. Lett.,* Vol. 32, 1518–1519, 1996.

13. Awan, S. A., S. Sail, C. M. Friend, and T. P. Beales, "Study of self-field AC losses in mono and multi-filament Bi-2223 tapes for power applications," *IEEE Trans. Appl. Supercond,* Vol. 7, No. 2, 335–338, 1997.

14. Brandt, E. H. and M. Indenbom, "Type-II-superconductor strip with current in a perpendicular magnetic field," *Phys. Rev. B,* Vol. 48, No. 17, 12893–12906, 1993.

15. Zeldov, E., J. R. Clem, M. McElfresh, and M. Darwin, "Magnetization and transport current in thin superconducting films," *Phys. Rev. B,* Vol. 49, No. 14, 9802–9822, 1994.

16. Awan, S. A., S. Sail, C. M. Friend, and T. P. Beales, "Self-field a.c. losses in mono- and multi-filamentary Bi-2223/Ag tapes at power frequencies," *Cryogenics,* Vol. 37, No. 10, 32–37, 1997.

17. Wilson, M. N., *Superconducting Magnets,* Oxford Press, 1989.

18. Forsyth, E. B., "Energy loss mechanisms of superconductors used in alternating-current power transmission systems," *Science,* Vol. 242, 391–399, 1988.

19. Müller, K. H. and K. E. Leslie, "Self-field ac loss of Bi-2223 superconducting tapes," *IEEE Trans. Appl. Supercond.,* Vol. 7, No. 2, 306–309, 1997.

20. Vellego, G. and P. Metra, "An analysis of the transport losses measured on HTSC single-phase conductor prototypes," *Supercond. Sci. Technol.,* Vol. 8, 476–483, 1995.